

### 3 STRONG GROUND MOTION OBSERVATIONS

This chapter discusses observed strong ground motions from the 14 November 2016  $M_w$ 7.8 Kaikoura earthquake. Specific attention is given to the near-source region where ground motions exceeding 1.0 g horizontal were recorded, as well as up to 2.7 g in the vertical direction at one location. Ground motion response spectra in the near-source, North Canterbury, Marlborough and Wellington regions are examined and compared with design levels. Observed spectral amplitudes are also compared with predictions from empirical and physics-based ground motion modelling.

#### 3.1 Tectonic setting and inferred causative rupture

Observations and multiple geophysical and geodetic methods highlight the source complexity of this earthquake with numerous fault segments rupturing (Litchfield et al., 2016; Stirling et al., 2017). Figure 3.1 illustrates the rupture segment geometries of the causative faults presented by Bradley et al. (2017b), and adopted here for ground motion observation and modelling interpretations. For reference, the surface trace of fault segments that are considered in the InSAR+GPS inversion of Hamling (2016), significant aftershocks, and mapped active faults are also shown.

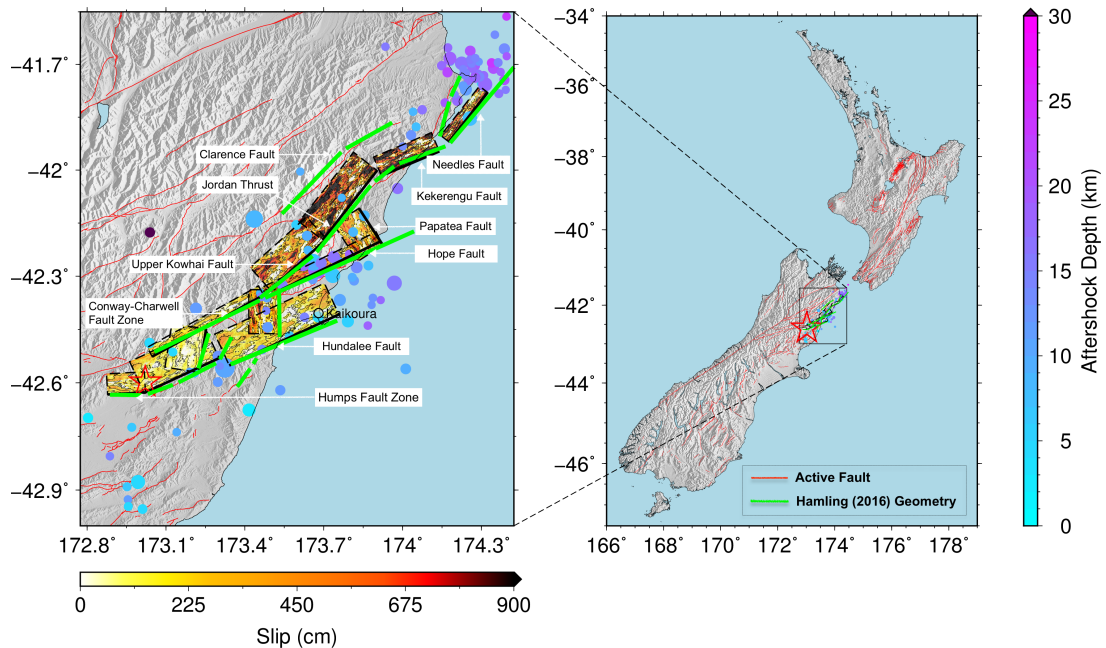


Figure 3.1: Location of the  $M_w$ 7.8 Kaikoura earthquake and causative faults on the east coast of the South Island, New Zealand. Hypocentre is marked with a red star. Surface trace of the source inversion of Hamling (2016) shown in green, and adopted kinematic rupture model faults shown as planes coloured by slip amplitude and contoured by rupture time.  $M_w > 4.5$  GeoNet CMT aftershocks till 15 Dec 2016 also illustrated as a function of centroid depth (after Bradley et al. (2017b)).

Litchfield et al. (2016) have so far identified at least nine fault segments (The Humps, Hundalee, Conway-Charwell, Upper Kowai, Fidget, Jordan Thrust, Papatea, Kekerengu, and Needles Faults) that have evidence of surface fault rupture. Eight of these faults are located onshore

with displacements obtained principally from direct field measurement of identifiable features; while rupture of the Needles Fault, located offshore at the northern end of the ruptured faults, has been identified from seabed uplift (NIWA, 2016). Most notably, essentially no surface rupture of the Hope Fault, the major fault identified *a priori* in the region (Stirling et al., 2012), has been mapped to date (Litchfield et al., 2016).

## 3.2 Ground motion observations

### 3.2.1 A regional view

A total of 224 Volume 1 (i.e. unprocessed) ground motion records were obtained from GeoNet, and processed to obtain realistic spectral ordinates over the vibration period range of  $T=0.01-10$  s, as discussed in Bradley et al. (2017b). Figure 3.2 illustrates the three component velocity time series of the GeoNet ground motion station recordings and their location relative to the causative rupture, which have a range in source-to-site distances of  $R_{rup}=0-216$  km. As would be expected, the highest velocities are evident in the near-source region. However, the nature of the waveforms vary significantly at similar  $R_{rup}$  values depending on the back-azimuth from the site to the rupture - those stations in proximity to the southern end of the rupture in North Canterbury (e.g., stations WTMC, WIGC, CULC, HSES, CECS) exhibit high-amplitude short-duration ground motions, while those at the north end of the rupture in northern Marlborough (e.g., SEDS, BWRS) and Wellington (e.g., FKPS, NEWS) have substantially longer duration and also well-defined multiple wave packets indicating delayed' rupture initiation of several segments. Central South Island stations, such as in Molesworth (MOLS) and Wairau Valley (WVFS), also exhibit two clear velocity wave packets.

Figure 3.3 illustrates the distribution of recorded geometric mean<sup>1</sup> peak ground acceleration,  $PGA$ . In total, 47, 16, and 5 ground motions were observed with  $PGA > 0.1$  g, 0.2 g, and 0.5 g, respectively, and will contribute substantially to the existing database of NZ strong motion records (e.g. Van Houtte et al., 2017). The subsequent sections discuss specific aspects of observed ground motions in regions of particular interest.

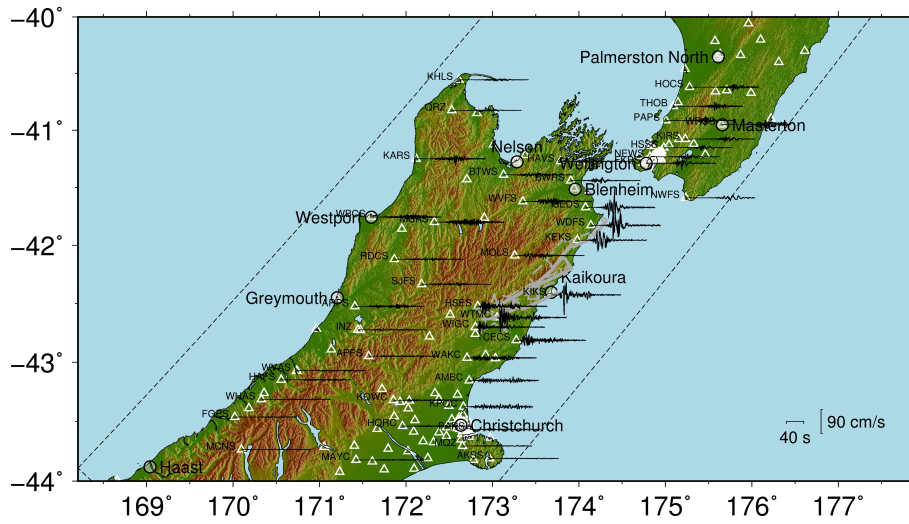
### 3.2.2 Accelerations in the near-fault region

Figure 3.4 illustrates four strong motion stations that are located in the immediate region of the causative faults. Station WTMC is located immediately near the inferred epicenter in Waiiau; KIKS in Kaikoura, approximately halfway along the north-south extent of the rupturing faults; and KEKS and WDFS are located in Kekerengu and Ward, respectively, at the northern end of the rupturing faults.

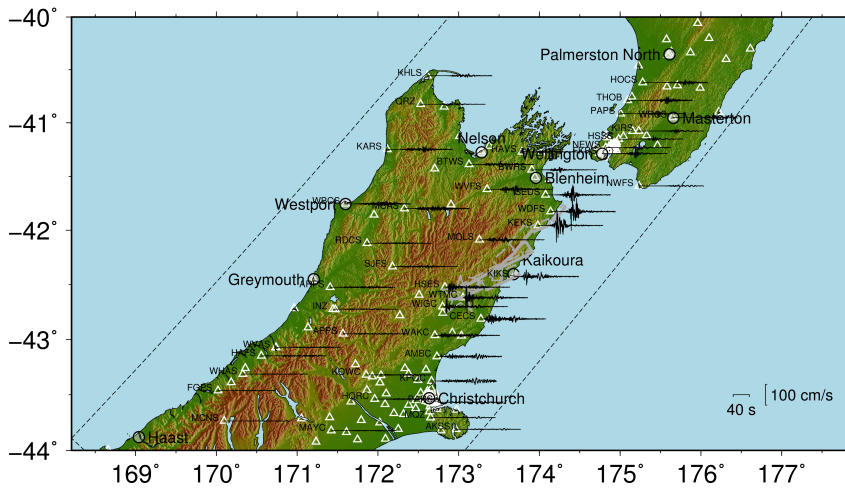
Because of its location near the epicenter (see Figure 3.1), the ground motion observed at WTMC (Figure 3.4a) indicates a short strong motion duration relative to the other three near-fault stations. The ground motion accelerations at WTMC exceed 1.0 g in both horizontal directions, and notably the acceleration in the vertical direction reaches 2.7 g (with a 100 Hz

---

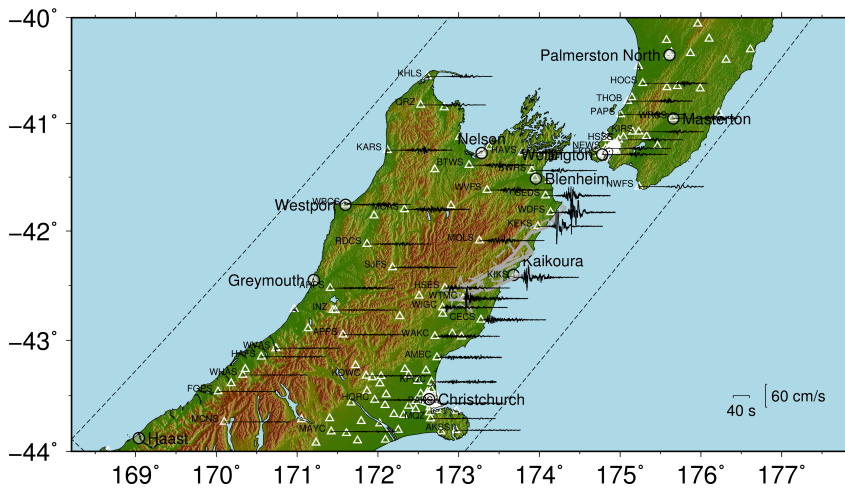
<sup>1</sup> Geometric mean metrics are used throughout unless noted.



(a) 000



(b) 090



(c) vertical

Figure 3.2: Spatial illustration of the variation in observed ground motion accelerations at selected strong motion stations for: (a) north-south (000); (b) east-west (090); and (c) vertical components.

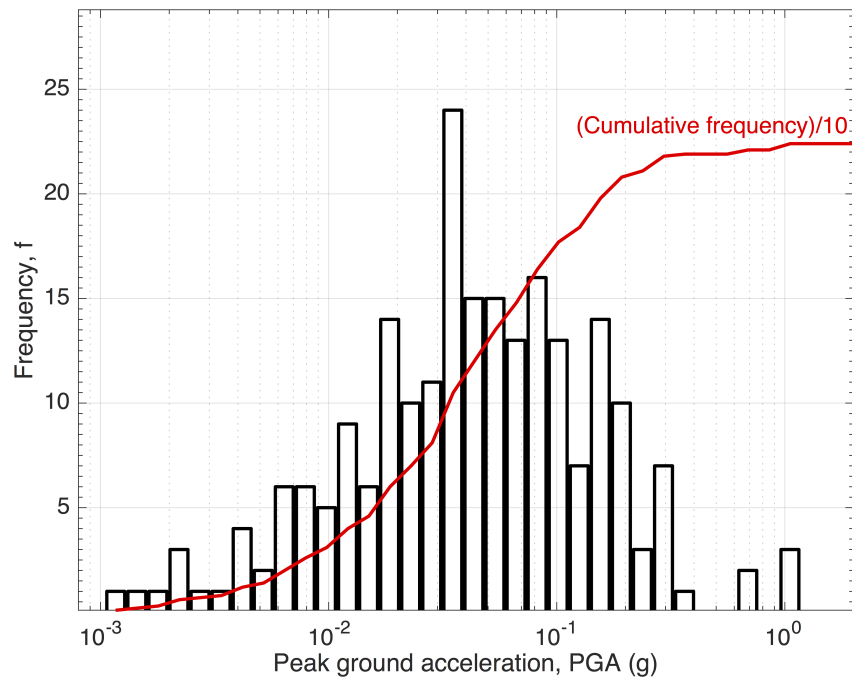


Figure 3.3: Distribution of geometric mean horizontal peak ground acceleration, PGA, recorded by strong motion stations (after Bradley et al. (2017b)).

high-cut filter). It is worth noting that the vertical accelerations exhibit strong asymmetry toward higher amplitudes in the positive direction (e.g., two exceedances of +2.0 g, while negative accelerations are limited to a little over -1.0 g). This phenomena has been documented in several ground motions from past earthquakes such as the 2011 Christchurch, New Zealand (Bradley and Cubrinovski, 2011; Fry et al., 2011), and the 2008 Iwate-Miyagi, Japan (Aoi et al., 2008; Yamada et al., 2009; Tobita et al., 2010) earthquakes. As demonstrated by Tobita et al. (2010) and Jeong and Bradley (2016), such asymmetry results from the varying near surface soil shear strength during induced compression and dilation. Furthermore, independent evidence of the extreme vertical accelerations in the vicinity of the WTMC site were seen in the form of bearing pads significantly moving (and, in one case, coming out from) between bridge abutment and girders at two bridges on Inland Road (SH70), within 2km from the WTMC station. Further information on this observed bridge damage is discussed in Chapter 6 of this report.

The KIKS station recorded relatively small levels of ground motion acceleration, given its location on a peninsula near the north-south mid-point of the rupturing fault segments, with horizontal and vertical peak accelerations of approximately 0.22 g and 0.27 g, respectively. The horizontal peak velocities are also a similarly small  $PGV=41-45$  cm/s, as compared to the other three stations in Figure 3.4 which generally have  $PGV >80$  cm/s (velocity time series at all four stations are shown in Figure 3.2).

Figure 3.4c and 3.4d illustrate the recorded ground motion accelerations at Kekerengu (KEKS) and Ward (WDFS) stations, which are located near the northern end of the rupturing faults, and are themselves located 16km apart. Both of these stations clearly illustrate acceleration records which are dominated by two predominant wave packets, one near  $t = 60s$ , and the other near

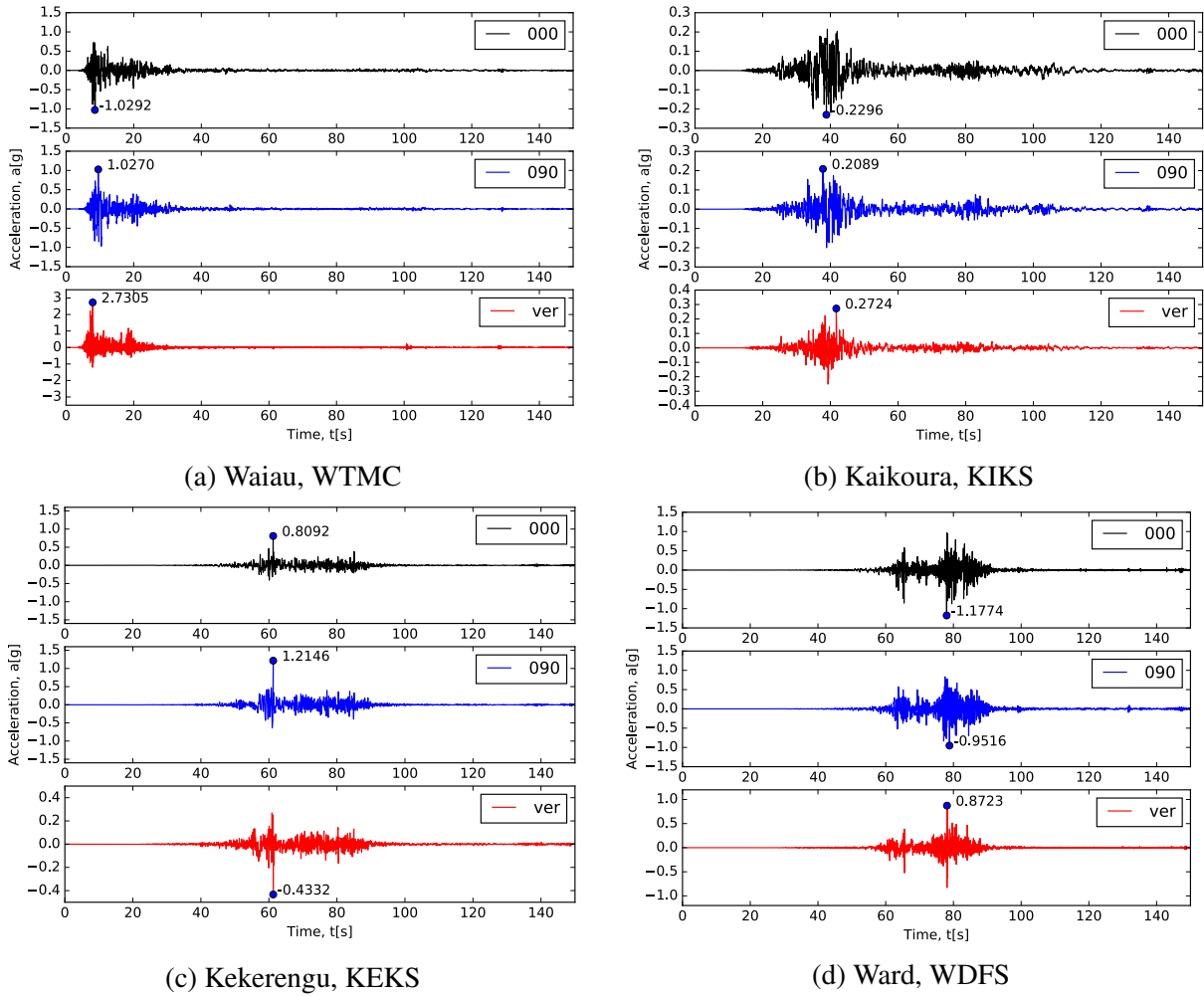


Figure 3.4: Recorded ground motion accelerations in the immediate vicinity of the rupturing faults (locations noted in Figure 3.2). 000, 090, and ver represent north-south, east-west and vertical components, respectively. Maximum accelerations in each component are explicitly noted. Different vertical axis scales are used for each station, and between horizontal and vertical components for clarity (after Bradley et al. (2017b)).

$t = 80s$ . Because of the fact that the KEKS station is within 2.5km of the mapped surface rupture of the Kekerengu fault (Litchfield et al., 2016) (with surface rupture displacements of 5-10m horizontal, and 1-2m vertical in the vicinity) it is reasonable to assume that the peak accelerations in the KEKS record correspond to the through-going rupture past this location. In contrast to KEKS, at the WDFS station the peak accelerations occur near  $t = 80s$ , which based on the source model in Figure 3.1 is inferred as the result of rupture of the Needles fault. Hamling (2016) inferred some (small) slip on the Grassmere fault located onshore from the Needles fault (and thus closer to the WDFS station). Further inferences of the source rupture from these observed ground motions are discussed in Bradley et al. (2017b).

### 3.2.3 Observed response spectra

Figure 3.5 illustrates the observed 5% damped (pseudo-acceleration) response spectra of stations in the near-fault region (i.e. Figure 3.4) as well as those in selected regions of North Canterbury, Marlborough, and Wellington. For reference, the site class C and D response spectra from NZS1170.5:2004 (NZS1170.5, 2004) for  $Z=0.4$  are also shown (it is acknowledged that the value of  $Z$  varies over the sites/regions illustrated, but a common value is depicted for consistent reference). At short vibration periods ( $T < 1s$ ) it can be seen that the largest response spectral amplitudes are observed in the near-fault region (Figure 3.5a) at the WTMC, KEKS, and WDFS stations, but also that large amplitudes are seen at the WIGC (Waiau Gorge) station in North Canterbury (Figure 3.5b) and SEDS (Seddon) station in Marlborough (Figure 3.5c). The short period ground motion amplitudes in Kaikoura and Wellington, other locations in North Canterbury and Marlborough, have appreciably smaller values as a result of the attenuation associated with larger source-to-site distances.

The shape of the response spectra in Wellington (Figure 3.5d) are appreciably different than those in the other regions, principally in relation to their predominance of long-period ground motion - the result of both the source-to-site distance (leading to small short period amplitudes, as noted above), but also basin and site response effects (as discussed in depth by Bradley et al. (2017a,b)).

### 3.3 Comparison of observations with ground motion modelling

Bradley et al. (2017b) provide further insights into the observed ground motions discussed in the previous section via comparison with empirical and physics-based ground motion modelling. Figure 3.6 illustrates snapshots of the simulated ground motion wavefield (in the form of ground motion velocity at the surface) for nine time instants during the simulation (A video is available at: <https://youtu.be/ZbI7rgnZ2U8>)<sup>2</sup> During the first 30 seconds of the simulation it can be seen that the 'southern' fault segments (The Humps, Hundalee, Hope) rupture in a northerly direction. Approximately at  $t = 40s$  the delayed rupture initiation at the southern end of the Jordan Thrust starts, and these 'northern' faults (Jordan, Kekerengu, Papatea, Needles) rupture over the following 40 seconds. Finally, after the rupture itself ceases at approximately  $t = 80s$ , the wavefield, with pronounced directivity migrating to the northeast, approaches the lower North Island.

Figure 3.7 provides a summary of the ground motion intensities over the simulation domain in the form of the peak ground acceleration,  $PGV$  (three-component maximum), and the Modified Mercalli Intensity (MMI) values, based on the MMI-to- $PGV$  correlation of Worden et al. (2012). As implied by the wavefield snapshots in Figure 3.6, it can be seen that significant directivity occurs to the north east as a result of the fault geometries and rupture sequence (fortunately a

---

<sup>2</sup> The waveform anomaly near Lon:174.5° Lat:-43.2° is the result of a discontinuity between the domain-wide model of Eberhart-Phillips et al. (2010), with the offshore portion of the Canterbury Velocity model of Lee et al. (2016). It is present only in the offshore region and the resulting localized spurious wavefield does not have a material effect on the simulated motion onshore.

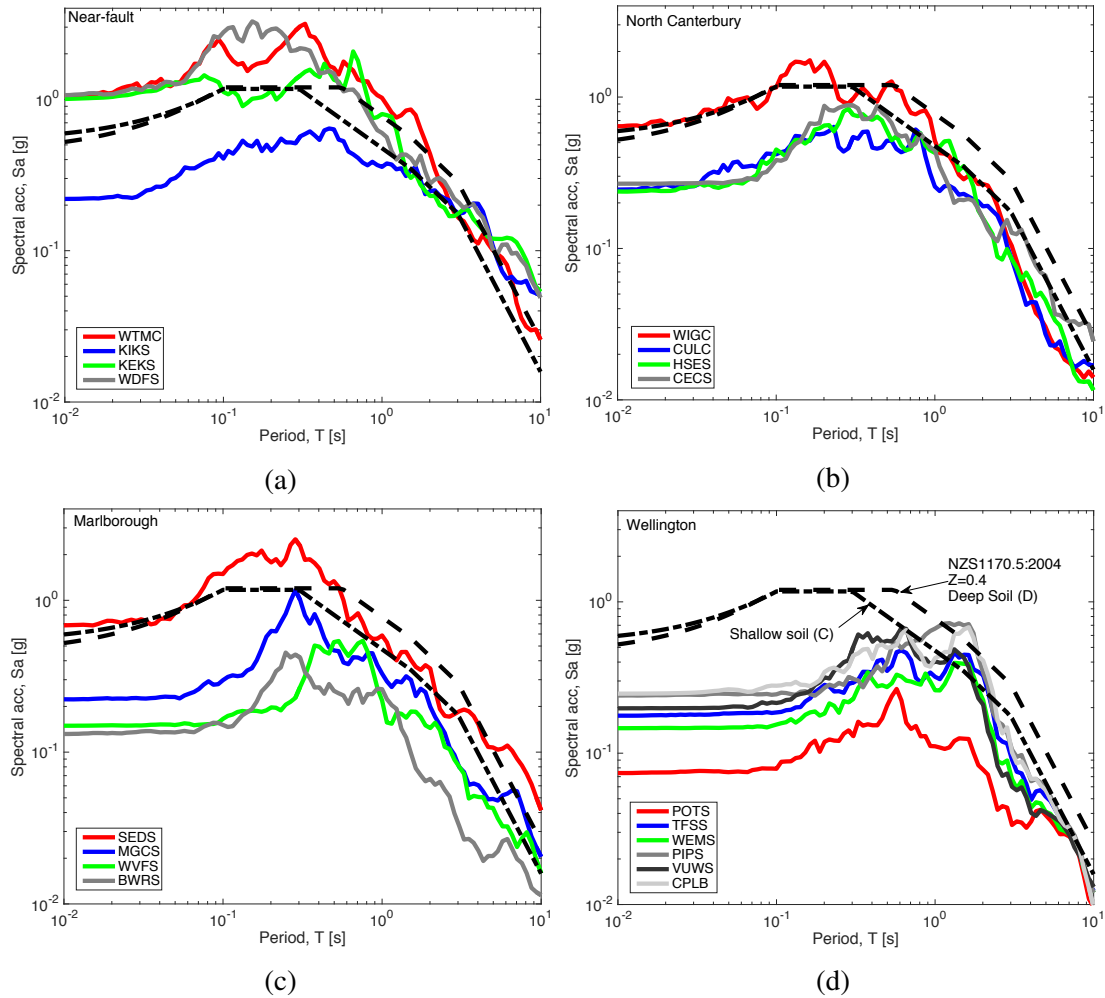


Figure 3.5: A regional depiction of the geometric mean horizontal 5% damped pseudo-acceleration response spectra observed in: (a) the near-fault; (b) North Canterbury; (c) Marlborough; and (d) Wellington. Four letter station codes in the figure legends can be located spatially in Figure 3.2

significant portion of the  $MMI > 8$  region occurs offshore, or in low-population density areas). As a result, the ground motion amplitudes to the south and west of the causative faults were modest in comparison. It can be seen that the Marlborough and Lower North Island was subject to approximately  $MMI = 7$  ground motion amplitudes with  $PGV = 20 - 40\text{cm/s}$ .

### 3.3.1 Comparison of response spectra modelling and observations

Figure 3.8 illustrates the observed and modelled ground motion spectral amplitudes for four vibration periods ( $T = 0.0, 0.2, 3.0,$  and  $10.0\text{s}$ ) as a function of source-to-site distance. The observed and simulated ground motion amplitudes for the 162 stations within the simulation domain are shown. The stations are also separately annotated based on their location in either the North or South Island. For reference, the NZ-specific empirical ground motion model of Bradley (2013) is also shown. It can be seen that the simulation provides a generally good comparison with the observed amplitudes. In particular, the distance attenuation in the observations

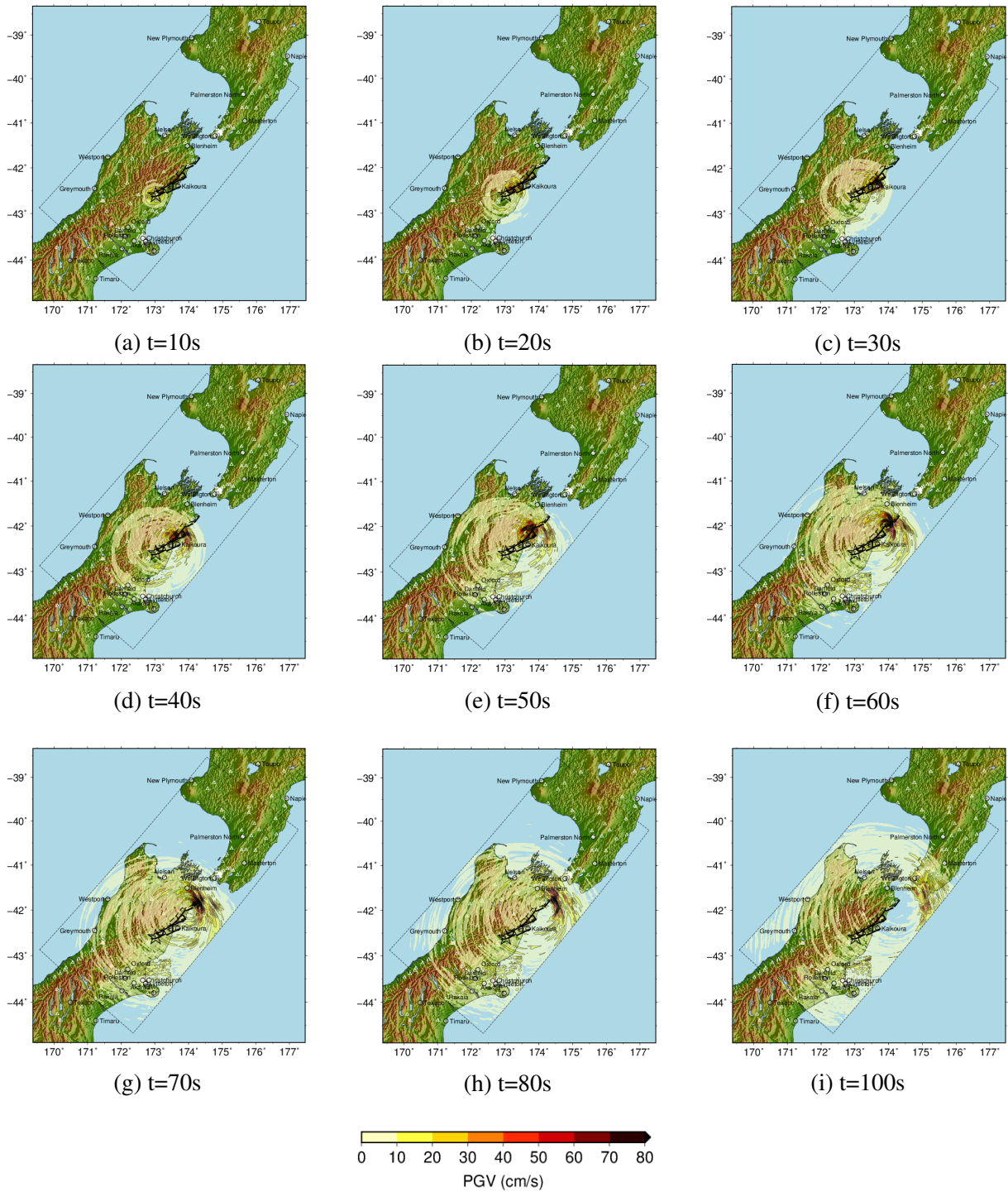


Figure 3.6: Time snapshots of simulated peak ground velocity (three component maximum). The causative fault segments and simulation domain are also indicated. A video of the simulation is available in the electronic supplement to this article and at: <https://youtu.be/ZbI7rgnZ2U8> (after Bradley et al. (2017b)).

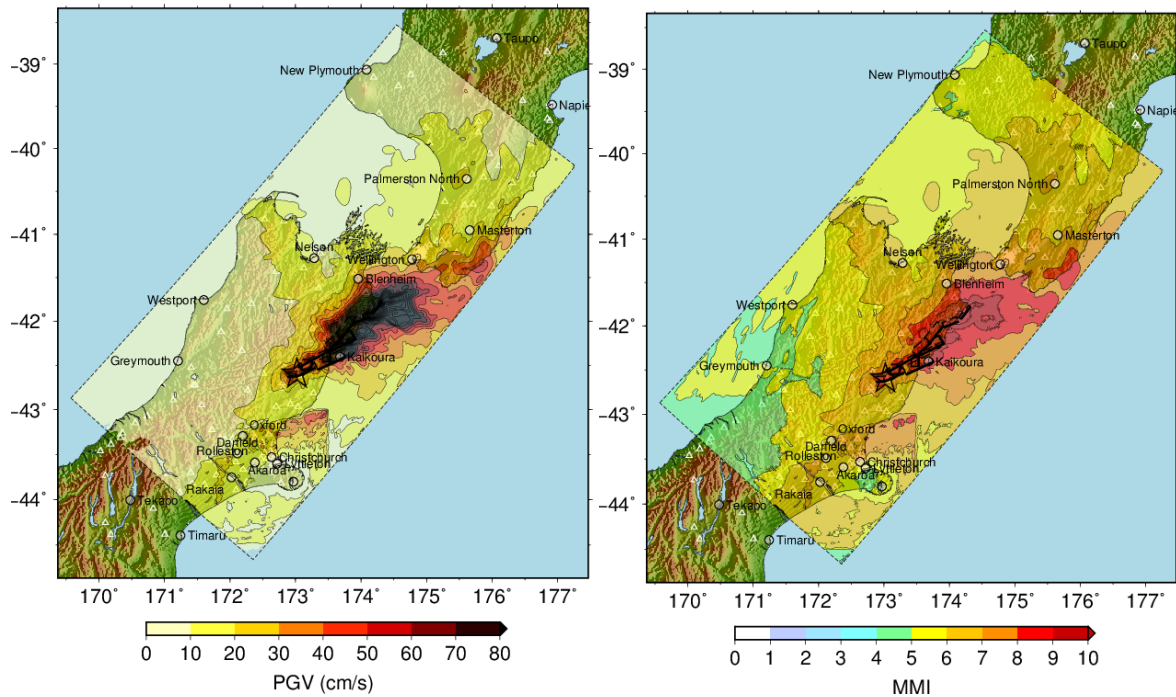


Figure 3.7: Spatial variation of: (a) peak ground velocity (PGV); and (b) Modified Mercalli Intensity (MMI) from the ground motion simulation (vector maximum of the two horizontal components).

at short periods (i.e.  $T = 0.0$  and  $0.2s$ ) is consistently predicted by the simulations, while the empirical model predicts a slower attenuation; conversely at long periods, the empirical model predicts a faster attenuation than exhibited by both the observed and simulated amplitudes. Although, not easily evident due to the large number of data points present, the simulations and observations are also broadly consistent in the higher-than-average amplitudes of North Island ground motions relative to those in the South Island for the same source-to-site distance, because of the aforementioned effect of rupture directivity. Bradley et al. (2017b) present further details on the predictive capabilities of the empirical and simulation-based methods.

### 3.4 Discussion

This chapter has provided a summary of observed ground motions from the 14 November 2016  $M_w 7.8$  Kaikoura earthquake. Ground motions were observed at over 200 strong motion stations, with 47 ground motions exceeding  $0.1 g$   $PGA$ . The strong motion dataset provide a significant complement to prior NZ strong motion data. The near-source ground motions clearly highlight the complexity of the earthquake rupture, with multiple wave packets in time clearly evident, and several very large horizontal and vertical amplitudes recorded. The response spectra of observed ground motions illustrated regions with large short and long period ground motion amplitudes. The long period amplitudes in Wellington are of particular note as discussed further in Bradley et al. (2017a).

Despite the rupture complexity of this event, the observed ground motions are broadly consistent with ground motion modelling. Short period ground motion amplitudes are well approximated

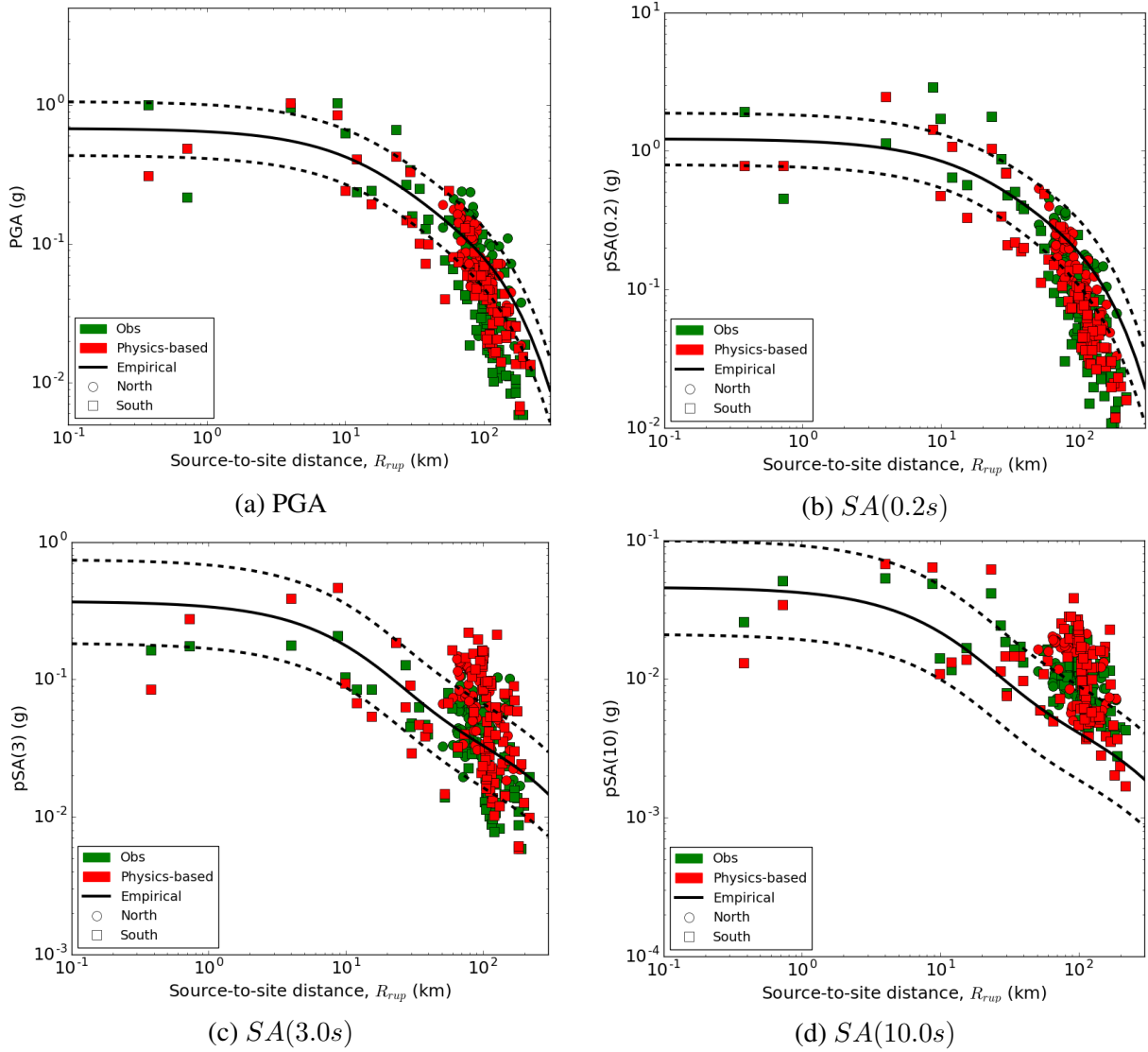


Figure 3.8: Observed, simulated, and empirically-predicted geometric mean 5% damped response spectra as a function of source-to-site distance,  $R_{rup}$ . Symbol shape indicates location of the station in the North or South Island. The median, and 16<sup>th</sup>/84<sup>th</sup> percentiles of the empirical prediction Bradley (2013) are represented by solid and dashed lines, respectively (after Bradley et al. (2017b)).

by empirical and simulation models, although the observations (and simulation modelling) indicate greater attenuation at larger distances ( $R_{rup} > 60km$ ) than in empirical modelling. Long period ground motion amplitudes are, on average, well approximated by the simulation-based modelling, and exceed empirical models at long vibration periods. A strong directivity is seen in the long period spectral amplitudes, with larger values at sites located in the general northward direction from the causative faults. Such directivity is captured to some extent in the simulations, but not accounted for in the particular empirical model used (although there are directivity modification models for empirical prediction developed by others).

## References

- Aoi, S., Kunugi, T., and Fujiwara, H. (2008). “Trampoline effect in extreme ground motion.” *Science*, 322(5902), 727–730.
- Bradley, B. A. (2013). “A new zealand-specific pseudospectral acceleration ground-motion prediction equation for active shallow crustal earthquakes based on foreign models.” *Bulletin of the Seismological Society of America*, 103(3), 1801–1822.
- Bradley, B. A. and Cubrinovski, M. (2011). “Near-source strong ground motions observed in the 22 February 2011 Christchurch earthquake.” *Seismological Research Letters*, 82(6), 853–865.
- Bradley, B. A., Wotherspoon, L. M., and Kaiser, A. E. (2017a). “Ground motion and site effect observations in the Wellington region from the 2016 Mw7.8 Kaikōura, New Zealand earthquake.” *Bulletin of the New Zealand Society for Earthquake Engineering*, 50(2), 94–105.
- Bradley, B. A., Razafindrakoto, H. N. T., and Polak, V. (2017b). “Ground motion observations from the 14 November 2016 Mw7.8 Kaikōura, New Zealand earthquake and insights from broadband simulations.” *Seismological Research Letters*, (DOI: 10.1785/0220160225).
- Eberhart-Phillips, D., Reyners, M., Bannister, S., Chadwick, M., and Ellis, S. (2010). “Establishing a Versatile 3-D Seismic Velocity Model for New Zealand.” *Seismological Research Letters*, 81(6), 992–1000.
- Fry, B., Benites, R., and Kaiser, A. (2011). “The character of accelerations in the Mw6.2 Christchurch earthquake.” *Seismological Research Letters*, 82(6), 846–852.
- Hamling, I. (2016). “Preliminary source inversion of the 14 November 2016 Mw7.8 Kaikōura earthquake (personal communication).
- Jeong, S. and Bradley, B. A. (2016). “Simulation of strong asymmetrical vertical acceleration at Heathcote Valley in the 2010-2011 Canterbury earthquakes.” *New Zealand Society for Earthquake Engineering Annual Conference*.
- Lee, R., Bradley, B., Ghisetti, F., and Thomson, E. (2016). “Development of a 3D high-resolution velocity model for the Canterbury, New Zealand region.” *Bulletin of the Seismological Society of America (submitted)*.
- Litchfield, N. J., Benson, A., Bischoff, A., Hatem, A., Barrier, A., Nicol, A., Wandres, A., Lukovic, B., Hall, B., Gasston, C., Asher, C., Grimshaw, C., Madugo, C., Fenton, C., Hale, D., Barrell, D., Heron, D., Strong, D., Townsend, D., Nobe, D., Howarth, J., Pettinga, J., Kearse, J., Williams, J., Manousakis, J., Mountjoy, J., Rowland, J., Clark, K., Pedley, K., Sauer, K., Berryman, K., Hemphill-Haley, M., Stirling, M., Villeneuve, M., Cockroft, M., Khajavi, N., Barnes, P., Villamor, P., Carne, R., Langridge, R., Zinke, R., Van Dissen, R.,

- McCull, S., Cox, S., Lawson, S., Little, T., Stahl, T., Cochran, U., Toy, V., Ries, W., and Juniper, Z. (2016). "14th November 2016 M7.8 Kaikoura Earthquake. Preliminary surface fault displacement measurements. Version 2. GNS Science. <http://dx.doi.org/10.21420/G2J01F> .
- NIWA (2016). "Scientists detect huge fault rupture offshore from Kaikoura" <https://www.niwa.co.nz/news/scientists-detect-huge-fault-rupture-offshore-from-kaikoura> 22 November 2016 (last accessed 20 Dec 2016).
- NZS1170.5 (2004). *Structural design actions, Part 5: Earthquake actions - New Zealand*. Standards New Zealand.
- Stirling, M., McVerry, G., Gerstenberger, M., Litchfield, N., Van Dissen, R., Berryman, K., Barnes, P., Wallace, L., Villamor, P., Langridge, R., Lamarche, G., Nodder, S., Reyners, M., Bradley, B., Rhoades, D., Smith, W., Nicol, A., Pettinga, J., Clark, K., and Jacobs, K. (2012). "National seismic hazard model for New Zealand: 2010 update." *Bulletin of the Seismological Society of America*, 102(4), 1514–1542.
- Stirling, M. W., Litchfield, N. J., Villamor, P., Van Dissen, R. J., Nicol, A., Pettinga, J., Barnes, P., Langridge, R. M., Little, T., Barrell, D. J. A., Mountjoy, J., Ries, W. F., Rowland, J., Fenton, C., Hamling, I., Asher, C., Barrier, A., Benson, A., Bischoff, A., Borella, J., Carne, R., Cochran, U., M., C., Cox, S. C., Duke, G., Fenton, F., Gasston, C., Grimshaw, C., Hale, D., Hall, B., Hao, K., Hatem, A., Hemphill-Haley, M., Heron, D., Howarth, J., Juniper, Z., Kane, T., Kearse, J., Khajavi, N., Lamarche, G., Lawson, S., Lukovic, B., Madugo, C., Manousakis, I., McColl, S., Noble, D., Pedley, K., Sauer, K., Stahl, T., Strong, D., Townsend, D. B., Toy, V., Villeneuve, M., Wandres, A., Williams, J., Woelz, S., and Zinke, R. (2017). "The Mw7.8 2016 Kaikōura earthquake: Surface fault rupture and seismic hazard context." *Bulletin of the New Zealand Society for Earthquake Engineering*, 50(2), 73–84.
- Tobita, T., Iai, S., and Iwata, T. (2010). "Numerical analysis of near-field asymmetric vertical motion." *Bulletin of the Seismological Society of America*, 100(4), 1456–1469.
- Van Houtte, C., Bannister, S., Holden, C., Bourguignon, S., and McVerry, G. (2017). "The New Zealand strong motion database." *Bulletin of the New Zealand Society for Earthquake Engineering*, 50(1), 1–20.
- Worden, C. B., Gerstenberger, M. C., Rhoades, D. A., and Wald, D. J. (2012). "Probabilistic relationships between ground-motion parameters and Modified Mercalli Intensity in California." *Bulletin of the Seismological Society of America*, 102(1), 204–221.
- Yamada, M., Mori, J., and Heaton, T. (2009). "The slapdown phase in high-acceleration records of large earthquakes." *Seismological Research Letters*, 80(4), 559–564.